VenSAR on EnVision: taking Earth Observation radar to Venus

Richard C. Ghail

Imperial College London, Civil and Environmental Engineering, London, SW7 2AZ, United Kingdom

r.ghail@imperial.ac.uk

David Hall

Airbus Defence and Space – Space Systems, Anchorage Road, Portsmouth, Hampshire PO3 5PU, United Kingdom

Philippa J. Mason

Imperial College London, Earth Science and Engineering, London, SW7 2AZ, United Kingdom

Robert R. Herrick

Geophysical Institute, University of Alaska Fairbanks, 903 Koyukuk Dr., Fairbanks, AK 99775-7320, United States of America

Lynn Carter

Lunar and Planetary Laboratory, The University of Arizona, 1629 E. University Blvd, Tucson, AZ 85721, United States of America

Ed Williams

Airbus Defence and Space – Space Systems, Anchorage Road, Portsmouth, Hampshire PO3 5PU, United Kingdom

Abstract

Venus should be the most Earth-like of all our planetary neighbours: its size, bulk composition and distance from the Sun are very similar to those of Earth. How and why did it all go wrong for

Venus? What lessons can be learned about the life story of terrestrial planets in general, in this era of discovery of Earth-like exoplanets? Were the radically different evolutionary paths of Earth and Venus driven solely by distance from the Sun, or do internal dynamics, geological activity, volcanic outgassing and weathering also play an important part? EnVision is a proposed ESA Medium class mission designed to take Earth Observation technology to Venus to measure its current rate of geological activity, determine its geological history, and the origin and maintenance of its hostile atmosphere, to understand how Venus and Earth could have evolved so differently. EnVision will carry three instruments: the Venus Emission Mapper (VEM); the Subsurface Radar Sounder (SRS); and VenSAR, a world-leading European phased array synthetic aperture radar that is the subject of this article. VenSAR will obtain images at a range of spatial resolutions from 30 m regional coverage to 1 m images of selected areas; an improvement of two orders of magnitude on Magellan images; measure topography at 15 m resolution vertical and 60 m spatially from stereo and InSAR data; detect cm-scale change through differential InSAR, to characterise volcanic and tectonic activity, and estimate rates of weathering and surface alteration; and characterise of surface mechanical properties and weathering through multi-polar radar data. These data will be directly comparable with Earth Observation radar data, giving geoscientists unique access to an Earth-sized planet that has evolved on a radically different path to our own, offering new insights on the Earth-sized exoplanets across the galaxy.

1. Venus, our Prodigal Twin

Surprisingly little is known about our nearest planetary neighbour, not even the basic sequence and timing of events that formed its dominant surface features. NASA's 1989-1994 Magellan mission provided a global image of the surface at 100 – 200 m resolution, comparable in coverage and resolution to that of Mars after the Viking missions in the 1970s. Magellan revealed an enigma: a relatively young surface, rich in apparent geological activity, but with a crater distribution indistinguishable from random (Figure 1). The initial conclusion was that a global catastrophe half a billion years ago had resurfaced the planet: Venus was solved. After Viking, Mars was similarly thought to be understood, with everything known that needs to be known.

Two decades later, Pathfinder reignited public and scientific enthusiasm in Mars and since then newer and higher resolution data from MGS, MRO and Mars Express have revolutionised our understanding of current and past processes alike.

Figure 1 Global Crater Distribution

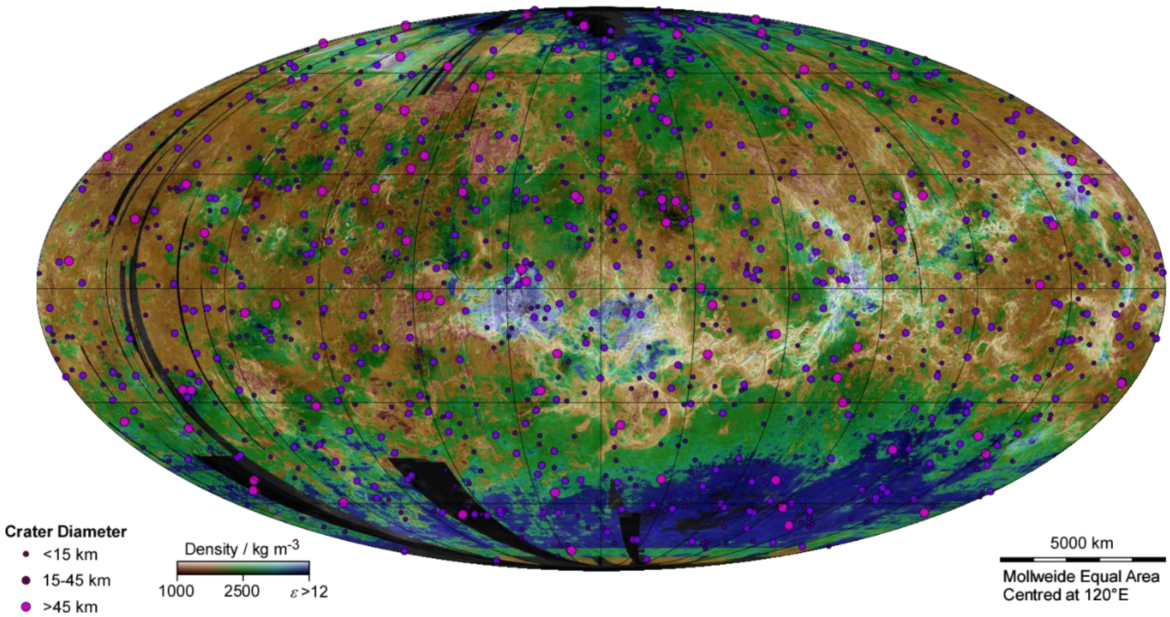

That the spatial distribution of impact craters is indistinguishable from a random is a puzzle because no other features on Venus occur at random. Underlying colour map shows surface materials: pink – loose sediment; brown – sedimentary or weathered rock; green – volcanic rock; blue – low permittivity materials.

ESA's 2006-2014 Venus Express, the most successful mission to Venus in the last two decades, revealed a far more dynamic and active planet than expected, uncovering tantalising evidence for present day volcanic activity that demands further investigation (Svedhem et al. 2007). Nonetheless, the enigma remains: how can a geologically active surface be reconciled with the global stasis inferred from the apparently random impact crater distribution? The outstanding science goals are therefore to determine the level and nature of current geological activity and the sequence of geological events that generated its range of surface features; assess whether Venus once had oceans or was hospitable for life; and understand the organising geodynamic framework that controls the release of internal heat over the history of the planet. EnVision builds on Europe's experience and technology heritage in Earth Observation to take a comprehensive look at our nearest planetary neighbour in unprecedented detail.

1.1. Geology, but not as we know it

Observations from Magellan data imply a variety of age relationships and long-term activity (Chetty et al. 2010; DeShon et al. 2000), with at least some activity in the recent past (Ghail 2002a; Price et al. 1996; Smrekar et al. 2010a). There is a non-random distribution of topography (the highs particularly are semi-linear features) and an association between geological features and elevation, such that the uplands are consistently more deformed than the lowlands. The distribution of impact craters is not strictly random either (Campbell 1999; Hauck et al. 1998; Price et al. 1996), with recent observations about the degree of crater alteration (Herrick and Rumpf 2011) permitting a wider range of possible recent geological activity (Campbell 1999; Guest and Stofan 1999; Hansen and Young 2007; Johnson 2003; Stofan et al. 2005).

Steep slopes and landslides are very common on Venus, implying active uplift, but existing data provide no constraint on current rates of tectonic activity. The surface of Venus is not organised into large plates like Earth's oceans but it is partitioned into areas of low strain bounded by narrow margins of high strain, analogous to continental basins and microplates. Are these regions actively created and destroyed, like Earth's oceans, or simply mobilised locally? What is the significance of the global network of elevated rift systems (Figure 2), similar in extent to mid-ocean ridges but very different in appearance? Unique to Venus are coronae, quasi-circular tectonic features, typically 100–500 km across, with a range of associated volcanic features. Are coronae the surface expression of plumes or magmatic intrusions? What role do they play in global tectonic and volcanic change?

Figure 2 Volcanic and Tectonic Features

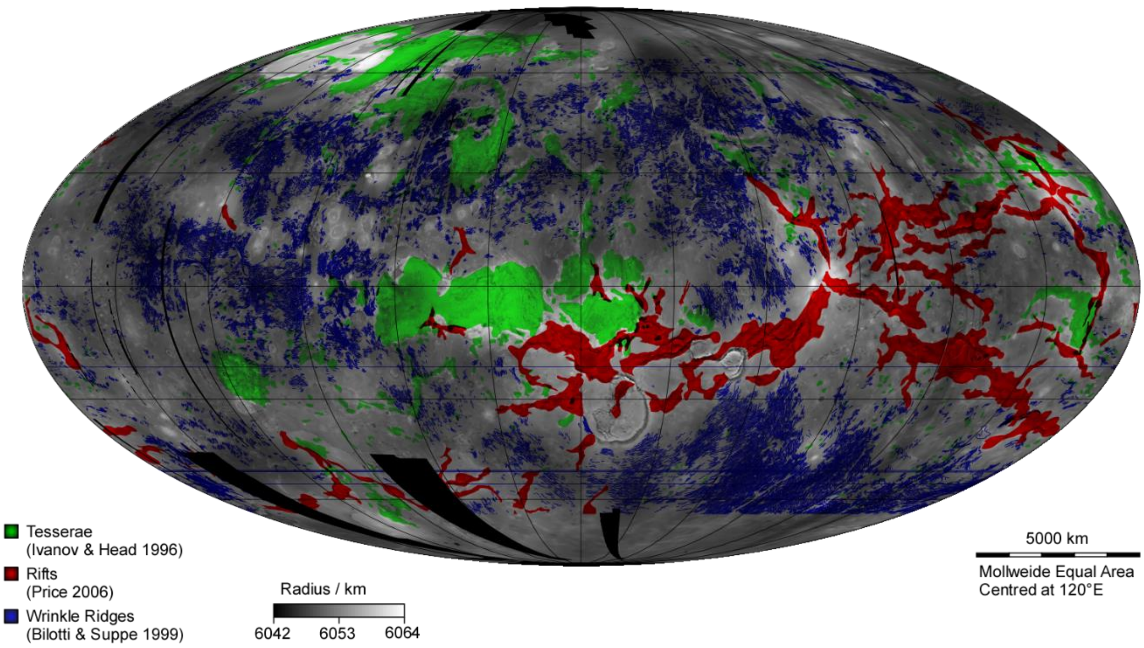

Rifts follow topographic rises along great circle arcs, similar to Earth's mid-ocean ridges; wrinkle ridges are predominantly in the lowlands. Tesserae are highly deformed terrain across a range of elevations, and are possibly continental crust.

Recent and perhaps ongoing volcanic activity has been inferred in both Venus Express (Marcq et al. 2013; Shalygin et al. 2014; Smrekar et al. 2010c) and Magellan (Bondarenko et al. 2010) data. Maintenance of the clouds requires a constant input of H_2O and SO_2 (Bullock and Grinspoon 1996) which equates to a magma effusion rate of only $0{\cdot}5$ km^3 a^{-1}, assuming a saturated magma source.

However, only one significant volatile-rich pyroclastic flow deposit, Scathach Fluctus (Ghail and Wilson 2013), has been identified to date, and the morphology of most larger volcanoes is consistent with low volatile eruptions. The actual magmatic rate is likely far higher, ~10 km^3 a^{-1}, about one third Earth's (Grimm and Hess 1997).

Constraining volcanic activity is critical to understanding when and how Venus was resurfaced, but it is also important to constrain the nature of that activity. Are there other large pyroclastic eruptions or is Scathach Fluctus unique? Are canali or other specific magmatic features confined to a past regime or still active today? Is there a correlation between mesospheric SO_2

concentration and volcanic activity? Are crater floors effusively infilled and buried from below? Were the plains formed from a few massive outpourings in a short period of time or from many thousands of small flows over their entire history? Or were they formed, or modified, in an entirely different way?

1.2. Its hell down there

The slow moving dense lower atmosphere of Venus creates a sedimentary environment similar to the deep oceans on Earth, but at 735·3 K (Seiff et al. 1985). Dunes and other aeolian features are rarely large enough to be visible in Magellan images so new data to understand its modern sedimentary processes is key to distinguishing whether ancient deposits formed under similar conditions or under more benign water oceans. Surface images captured by Soviet Venera landers reveal a landscape more consistent with pyroclastic or sedimentary deposits, not the basaltic lava flows widely assumed to cover the plains. The bedrock recorded at the Venera 10, 13 and 14 sites consists of laminated or thinly bedded sheets with varying degrees of coarse sediment or regolith (Figure 3).

Figure 3 Venera Landing Sites

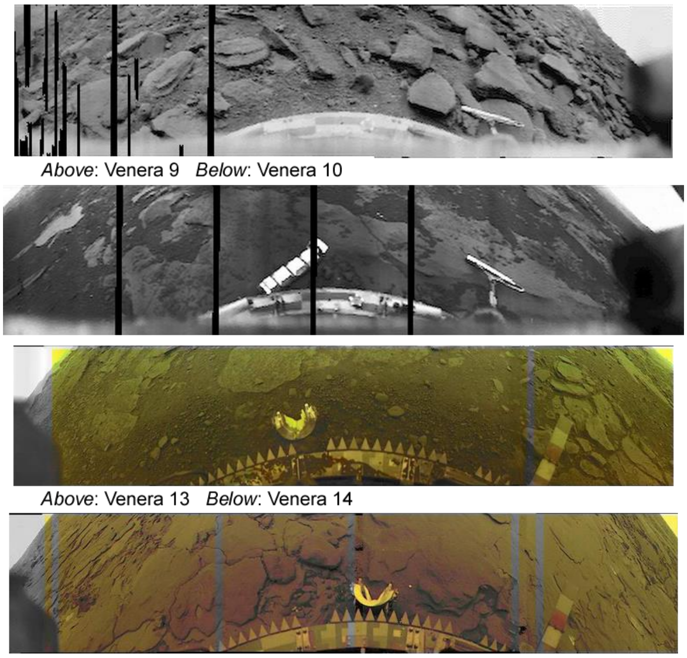

Venera 9 landed on a talus slope of about 30˚; Veneras 10, 13 and 14 landing on rolling plains with varying amounts of loose sediment and plate-like bedrock (Marov and Grinspoon 1998). Reprocessed lander image data © Don P. Mitchell, used with permission.

Although chemically similar to basalts, the layering is more similar to sedimentary or pyroclastic bedding (Florensky et al. 1983a), formed by cycles of air fall or ground flow. Based on load carrying capacities derived from the penetrometer and dynamic loads during lander impact (Marov and Grinspoon 1998; Surkov et al. 1984), the strength of the surface at the Venera 13 site is similar to that of a dense sand or weak rock. At the Venera 14 and Vega 2 sites the recorded strengths are higher but similar to that of a sedimentary sandstone and less than half that of an average basalt.

A major problem is that almost the entire area imaged by each Venera lander sits within a single Magellan SAR (Synthetic Aperture Radar) pixel, and their landing position is known to only ~150 km, so that it is impossible to correlate features observed in the lander images with those in Magellan images. Do the lander images represent a surface weathering veneer on otherwise intact lava flows, or thick accumulations of aeolian or pyroclastic deposits?

1.3. Where are the plates?

The lack of plate tectonic features such as spreading ridges and subduction zones; the close correlation between geoid and topography at both long and short wavelengths (Simons et al. 1994), unlike Earth; and the near random distribution of the ~940 impact craters on Venus, imply a stagnant lid regime (Armann and Tackley 2012; Reese et al. 1998, 1999; Solomatov and Moresi 1996) and a globally uniform surface age (McKinnon et al. 1997; Phillips et al. 1992; Strom et al. 1994) of ~750 million years. A proposed global stratigraphic sequence (Basilevsky and Head 1998; Ivanov and Head 2011) suggests rapid global resurfacing, probably episodic (Fowler and O'Brien 1996; Noack et al. 2012; Papuc and Davies 2012; Turcotte 1993; Turcotte et al. 1999), followed by a long period of quiescence. However, observations from Magellan data reveal an array of organised geological complexity (Anderson and Smrekar 2006; Ghail 2015; Jiménez-Díaz et al. 2015) implying a variety of age relationships and long-term activity (Chetty et al. 2010; DeShon et al. 2000), at least some of which was in the recent past (Ghail 2002b; Price et al. 1996; Smrekar et al. 2010b). There is a non-random distribution of topography (Ford and Pettengill 1992; Rappaport et al. 1999), deformation (Jurdy and Stefanick 1999; Stofan et al. 2001) and volcanism (Head et al. 1992); the distribution of impact craters is not strictly random either (Campbell 1999; Hauck et al. 1998; Price et al. 1996), with recent observations about the degree of crater alteration (Herrick and Rumpf 2011) permitting a wider range of possible recent geological activity (Guest and Stofan 1999; V.L. Hansen and Young 2007; Johnson 2003; Stofan et al. 2005). While tesserae on the highland plateaus and elsewhere may be the equivalent of continental crust on Earth, they cover only a quarter as much area and occur across a wider range of elevations, since Venus lacks Earth's bimodal topography (Bonin et al. 2002; Gilmore et al. 1998; Hashimoto et al. 2008; Ignacio Romeo et al. 2005; Romeo and Capote 2011; Shellnutt 2013).

The Venus surface appears to be partitioned into regions of relatively low strain surrounded by narrow belts of high strain (Figure 4) that we refer to as terranes, although we note that this term is used in a more general sense here than is usual in terrestrial geology. Terranes on Venus are typically only 500~1500 km across, the same order of magnitude as the ~800 km average crater spacing, and so are likely important in understanding both the crater distribution and global resurfacing processes.

Figure 4 Example Terranes in Lada Terra

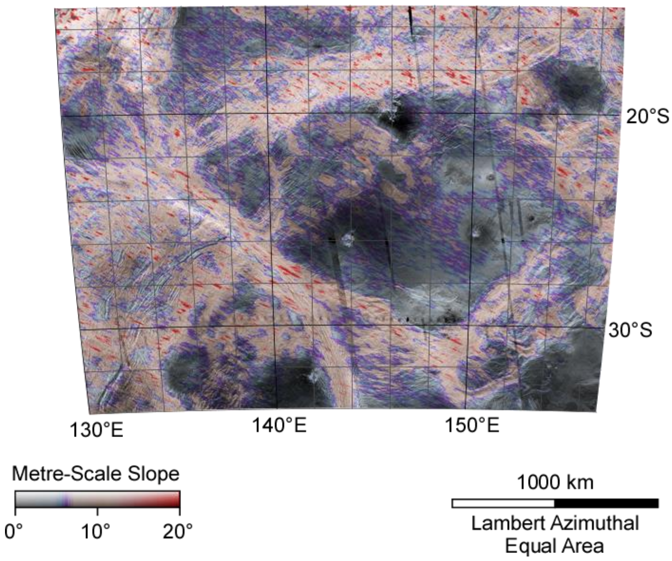

Magellan SAR image with false colour metre-scale slope as a proxy for strain, showing an average-sized tectonic terrane comprising an undeformed interior (blue) surrounded by relatively diffuse deformation belts (brown to red). Notice that these outline neighbouring terranes.

Terranes on Venus have a wide variety of morphologies ranging from, for example, the 600 km diameter Atete Corona to the 1500 km tessera plateau of Alpha Regio. Understanding their nature – how they are deformed and reworked – is therefore crucial to solving the paradox between the geological complexity of Venus and its crater distribution. What is the connection between these terranes and underlying mantle convection? How rapidly are the high strain margins being deformed and by what processes? What processes modify the low strain interiors and over what timescales? Are there distinct compositional differences between terranes? What is the relationship between terranes and volcanic processes? Addressing these questions requires a range of complementary observations to distinguish regionally-important geological formations and relationships.

2. Earth Observation, Version 2

EnVision is a proposed ESA Medium class mission to determine the nature and current state of geological activity on Venus, and its relationship with the atmosphere, to understand how Venus and Earth could have evolved so differently. It carries three instruments: the Venus Emission Mapper (VEM), an infrared emission mapping spectrometer used to identify surface mineralogies at 50 km resolution, exploiting the few infrared windows in the global cloud layer that limits practical observations of the Venus surface; the Subsurface Radar Sounder (SRS), a 10-30 MHz radar sounder for detecting near-surface stratigraphy and geologic contacts; and VenSAR, the primary instrument and only one capable of imaging the surface at metre-scale resolution, and which is the subject of this article.

Geological processes operate at all scales, as recognised in conventional mapping (McCaffrey et al. 2005). The mapping hierarchy adopted for EnVision (Table 1) differentiates processes that operate at, and affect, features at the different scales indicated, and requires a resolution at least 2-3 times finer to discriminate these features. The *Zonal*-scale 100–200 m resolution of Magellan imagery enables mapping of the global distribution of volcanoes, for example, but not their age relationships, which would require *Reconnaissance*-scale imaging to reveal the cross-cutting relationships between different flows.

Table 1 EnVision Mapping Hierarchy

	Global	***Zonal***	***Reconnaissance***	***Exploration***	***Locality***
Coverage	>95%	>95%	>20%	>2%	>0·2%
Unit Area	Global	2500 × 2500 km	1500 × 1500 km	100 × 100 km	5 × 5 km
Resolution	50 km	150 m	30 m	6 m	1 m
Feature Size	150 km	500 m	100 m	20 m	<4 m
Geomorphological Features					
Structures	Terra ‘continents’, Planitia		Chasmata, Dorsa	Folds, graben	Fault scarps

Volcanoes	Volcanic rises (Regio)	Volcanic edifices	Lava Flows	Flow textures
Sediments	'Featureless' plains	Parabolas, halos	Landslides	Dunes

Geological processes operate across a range of scales; while global metre-scale data would perhaps be ideal, the data volume would be prohibitive to return and analyse. Instead, a nested set of observations sampling decreasing areas at increasing resolution, are sufficient to characterise the processes involved, e.g. textures observable at the Locality (metre) scale help to understand flows at Exploration scale, which help to understand edifices at the Reconnaissance and rises at the Zonal and Global scales.

In Earth observations, the C-band ERS-1, ERS-2 and ENVISAT all provided 30 m resolution data (the latter also 150 m and 1000 m data). At X-band, COSMO-SkyMed offers 100 m, 30 m and 5 m stripmaps and 1 m spotlight images and TerraSAR-X/Tandem-X 3 m stripmaps and 1 m spotlight images. Sentinel-1 data are available from 5 m to 40 m resolution at C-band. Not only have these resolutions proved effective on Earth, adopting the same resolutions on Venus means that there will be a wealth of comparable data from Earth. NovaSAR will acquire 30 m and 6 m S-band stripmap imagery at the same frequency, providing data directly comparable with EnVision.

Conceptually, therefore, EnVision is designed to deliver nested data (Woodcock and Strahler 1987), from measurements of the gravity field, spin rate and axial wobble at the global-scale, to metre-scale observations of current rates of activity and stratigraphic relationships, and thence on to a selection of locality-scale snapshots to show how global change is effected, from the smallest scales upwards.

Many Earth Observation SARs operate in C-band (5·4 GHz) or X-band (9·6 GHz), frequencies that are not suited to the Venus atmosphere due to atmospheric losses. Laboratory measurements in a CO_2 atmosphere with 300 ppm SO_2 at 435 K and up to 92 bars (Steffes et al. 2015), observations of Venus atmospheric opacity at wavelengths of 3·1 cm, 10·6 cm and longer (Muhleman 1969), and more recent observational data at wavelengths between 1·3 and 22·6 cm (Butler 2001), lead to a reasonable approximation to the expected one-way atmospheric losses in dB as simply one tenth of the square of the frequency in GHz (Figure 5). For InSAR, relative phase shifts caused by variability in the concentration of sulphuric acid droplets in the clouds are more severe at shorter wavelengths. For these reasons a radar system operating in the S-band (15 to 7·5 cm, 2 to 4 GHz) or longer is desirable in terms of operating power, signal to noise performance and phase stability.

Figure 5 Opacity of the Venus atmosphere at radar wavelengths

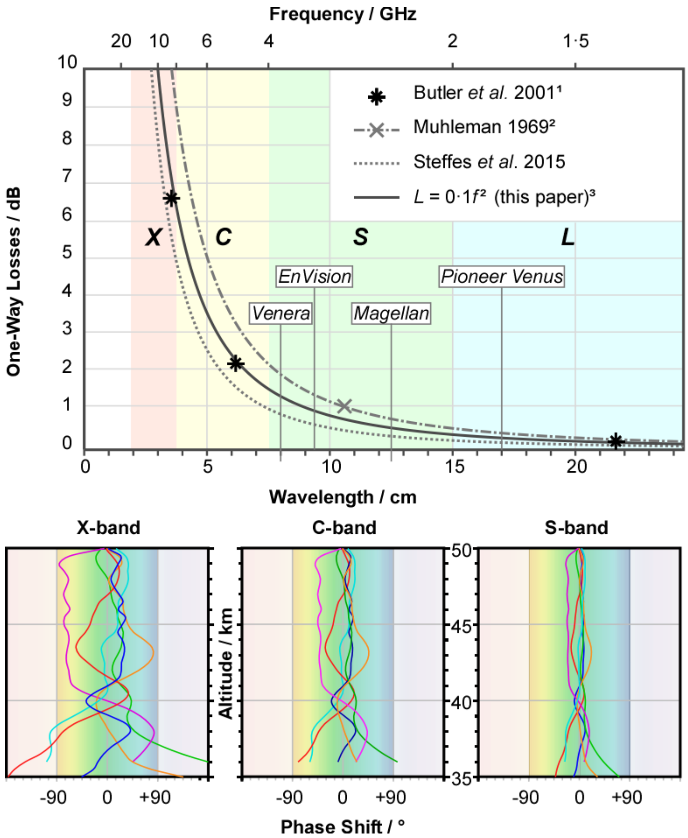

Top: *the opacity of the Venus atmosphere at radar wavelengths approximates a frequency squared dependence. Grey shading indicates complete loss of signal for practical purposes. Notes: [1]also 46·0 dB at 1·3 cm and 20·0 dB at 2·0 cm; [2]also 13 dB at 3·1 cm; and [3]L is the one-way loss in dB and f the frequency in GHz. The operating wavelengths of various radar systems are indicated.* Bottom: *relative phase shifts caused by changing concentrations of sulphuric acid cloud droplets in the cloud layer (based on Magellan occultation data) are excessive at shorter wavelengths.*

VenSAR is based on the NovaSAR-S instrument currently being built for the UK Space Agency and scheduled for launch in late 2016 / early 2017. NovaSAR-S is an active antenna is configured from an array of 18 identical phase centres each comprising a 2 × 2 array of dual polar, 6-element sub-arrays, designed for low-cost Earth Observations (Cohen et al. 2014) and operating at 3·2 GHz (9·4 cm) in the S-band, ideal for the Venus atmosphere. VenSAR adapts this modular design by taking 24 of these phase centres and configuring them into a six columns of four rows, producing a 5·47 × 0·60 m active phased array antenna capable of delivering five key science modes: InSAR (VI1 as standard, VI2 for orbit-to-orbit, and VI3 for opposite-look), stereo polarimetry (VP1 StereoPolSAR), all at *Reconnaissance* scale (30 m resolution); *Exploration* scale imagery (VH1 HiRes at 6 m resolution); *Locality*-scale Sliding Spotlight (VS1 Spotlight at 1 m resolution); and *Zonal*-scale microwave brightness temperature (VR1 Radiometry), summarised in Table 2.

Table 2 ***Summary of VenSAR operating mode parameters***

	Resolution	*Looks*	*Tx*	*Incidence*	*Sensitivity*	*Swath*	*Duration*	*Data*
VI1 InSAR	27 m	18	4%	21° – 31°	−21·8 dB	53 km	498 s	66 Mbps
VI2 InSAR	27 m	18	4%	19° – 29°	−20·9 dB	53 km	498 s	68 Mbps
VI3 InSAR	27 m	18	4%	−21° – −31°	−21·8 dB	53 km	498 s	66 Mbps
VP1 StereoPolSAR	30 m	9	4%	37° – 41°	−16·9 dB	53 km	873 s	127 Mbps
VH1 HiRes	6 m	6	20%	38° – 43°	−20·1 dB	22 km	291 s	353 Mbps
VH2 HiRes	6 m	6	20%	38° – 43°	−20·1 dB	32 km	291 s	513 Mbps
VS1 Spotlight	1 m	1	20%	38° – 39°	−21·5 dB	5 km	4 s	468 Mbps
VR1 Radiometry	5 × 30 km	n/a	0%	−4° – +4°	~1 K	38 km	<2760 s	<0·25 kbps

Note*: InSAR is here used to refer to stripmap swaths optimised for repeat-pass D-InSAR; in the strict sense, the first pass acquires SAR, the second InSAR, and the third D-InSAR. Resolution is given in the traditional sense of a point-spread function and not metres per pixel, as is usually the case for planetary cameras. SAR pixels are typically two-thirds the point-spread resolution, i.e. 4 m pixels for a 6 m resolution image; hence Magellan image pixels are 75 m for a resolution of ~110 m.*

3. Tools of the Trade

In normal stripmap SAR operations, the ultimate spatial resolution along track (azimuth) is nominally half the antenna length, ~3 m, while across track (range) it is controlled by the available RF bandwidth, which at 182 MHz is 1~2 m, depending on incidence angle. Radiometric resolution increases with the number of looks but at the expense of spatial resolution. A good compromise is ~9 looks (Woodhouse et al. 2011); Magellan images were typically only 5–6 looks in the lower latitudes. At high resolution, therefore, optimal images have 6 looks (2 in azimuth and 3 in range) and a spatial resolution of 6 m, suitable for Exploration scale mapping.

Operating at the full bandwidth has very high power demands (~2 kW at a 20% duty ratio) and data rates (~900 Mbits s^{-1}) that are not required for standard *Reconnaissance* mapping. By obtaining 9 looks in azimuth, the range resolution can be reduced to ~27 m, ideal for *Reconnaissance* mapping and requiring only ~15·5 MHz bandwidth, reducing the data rate to ~65 Mbits s^{-1} and the duty ratio to 4% (~600 W). These data have four times the spatial and three times the radiometric resolution of Magellan; at full resolution the spatial improvement is a factor of 20, for the same radiometric resolution as Magellan. In spotlight mode the spatial resolution is 120 times Magellan, at about half the radiometric resolution. All these modes have sufficient sensitivity to differentiate between different surface features on Venus (Figure 6).

Figure 6 **VenSAR mode sensitivities versus backscatter**

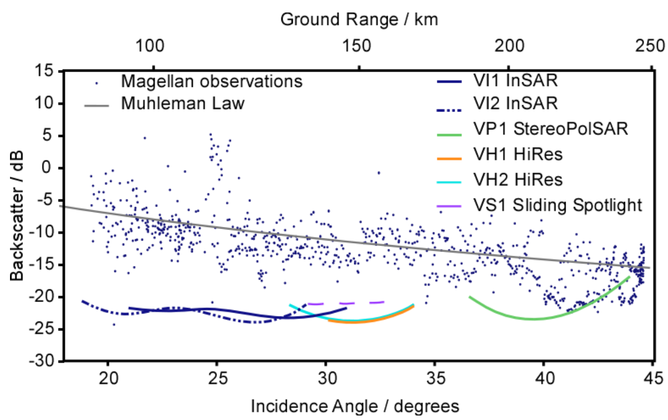

It is, however, possible to programme VenSAR for any other desired mode, incidence angle, or resolution, at any stage of the mission, making it a highly responsive system, but the nominal mission plan uses repeated daily blocks, with the same pre-defined operation modes to observe different targets, in order to minimise operations complexity. For each mode the radar antenna will be physically pointed towards the optimum illumination angle for each swath by rotation of the whole spacecraft about its roll axis, with beam shaping used only to optimise imaging performance.

3.1. 27 m Reconnaissance Interferometry Stripmap

Differential InSAR, or DInSAR, (Massonnet et al. 1993) is the only tool capable of measuring geological-scale strains from orbit and is particularly effective across high strain rate terrane margins, in which line of sight (LoS) displacements may be 10 mm a^{-1} or more. Combining LoS displacements derived from DInSAR sets in ascending and descending (opposite look) orbits allows the vertical and at least one of the horizontal components of displacement to be isolated (Hu et al. 2014; Wright 2004). Two complementary methods (Berardino et al. 2002; Ferretti et al. 2001) are commonly used to detect displacements as small as 1 mm a^{-1}, even in the absence of an earthquake (Lanari et al. 2007). Combining these techniques with opposite look sets to isolate components of movement means that even the low strain deformation of terrane interiors is detectable with DInSAR (Ghail et al. 2015; Mason et al. 2015).

Many fracture sets visible in Magellan images appear to have formed in response to subsurface dykes (McKenzie et al. 1992; Parfitt and Head 1993), which often occur in swarms that radiate in patterns related to the global stress state of the lithosphere (Grosfils and Head 1994). Coronae (Barsukov et al. 1986) – unique to Venus – also appear to be the surface expression of subsurface intrusions or magmatic plumes (Stofan et al. 1991) and recent research (Mikhail 2016) suggests that intrusions may be more important on Venus than Earth because its weak lower crust (Arkani-Hamed 1993) inhibits extrusion (Maccaferri et al. 2011). DInSAR is highly effective at detecting magmatic inflation under terrestrial volcanoes (Biggs et al. 2009; Fournier et al. 2010), even where no volcanic feature is evident (Wicks et al. 2006), making it the ideal tool to study magmatic processes associated with terrane margins and interiors. DInSAR may therefore reveal whether different rift morphologies and corona associations are related to an increased rate of subcrustal stretching and intrusive magmatism (Ghail 2015) or to different rift ages (Nagasawa et al. 1998; Smrekar et al. 2010a), and hence illuminating the details of the connections between surface features and underlying mantle processes.

For a short period between Cycles 1 and 2 (i.e. between the first and second sidereal rotation period of 243 days), Magellan was instructed to extend the radar burst duration across the North Pole of Venus to test for the viability of obtaining interferometric data. The results demonstrate that the atmosphere of Venus is stable over periods of at least 7½ hours (Figure 7). From a 259 km altitude circular polar orbit, EnVision will acquire two sets of interferometric SAR data, VI1 and VI2, in Stripmap mode (a continuously imaged swath), with the second stripmap ~90 minutes after the first, on the following orbit. During the delay between these two passes, Venus' slow rotation will cause the ground tracks of the two passes to be displaced from each other by 10 km at the equator.

Figure 7 **Magellan interferogram of the Venus North Pole**

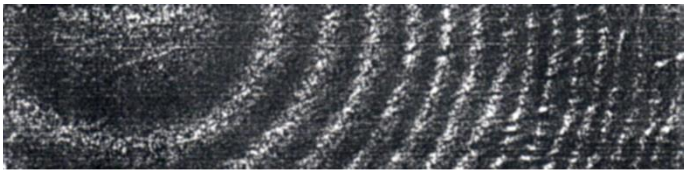

Goldstein, pers. comm.

This baseline would be too large to maintain coherence between these images using a common carrier frequency, but shifts in the carrier frequency between the two acquisitions enable the two data sets to be brought back into coherence (Gatelli et al. 1994; Meyer and Sandwell 2012). The required frequency shifts are on the order of 150 MHz and lie comfortably within the operating spectrum of the radar technology. The long spatial baseline increases the ratio of the topographic phase signal to atmospheric artefacts and other noise, improving the vertical resolution of the topographic model (DEM) produced. Orbit to orbit interferometry ensures that this baseline DEM is obtained within the first Cycle of the mission.

From the second Cycle onwards, EnVision will acquire VI1 and VI3 InSAR on consecutive orbits. VI1 will provide left-looking, and VI3 right-looking, repeat pass (Cycle-to-Cycle) coverage so that the east-west and vertical components of ground displacement may be resolved by comparing the line-of-sight changes in each D-InSAR stack (Mason et al. 2015). It is not possible to resolve the north-south component from a polar orbit but it can be inferred from the geological context (Ghail et al. 2015).

Coherence, a by-product of DInSAR, is also useful for change detection (Touzi et al. 1999): a reduction or loss of coherence implies change at the scale of the radar wavelength or above. Atmospheric effects, particularly changes in the cloud layers, are the primary factor in loss of coherence but are long wavelength features (at least 50 km) that can be corrected for (Ding et al. 2008). Surface changes causing coherence loss are usually smaller in scale and geographically distinct, often in the form of channels and lobate downslope mass movements (Schepanski et al. 2012). Canali are river-like channels thought to be formed by carbonatite or sulphur-rich volcanic flows (Kargel et al. 1994; Komatsu et al. 2001; Williams-Jones et al. 1998) or sedimentary density currents (Waltham et al. 2008); coherence data will distinguish between these possibilities from their pattern of coherence loss. Mass wasting (Florensky et al. 1977) and landslides are common on Venus (Malin 1992) and may contribute to a small but global supply of sediment, revealed in Magellan Doppler Centroid data (Bondarenko et al. 2006) and Venera lander images (Florensky et al. 1983b). Thus the pattern of coherence loss can reveal other mechanisms of surface change in addition to those from tectonic or volcanic processes.

Coherence and DInSAR change detection only reveal current rates and styles of activity and not whether these are in a long-term steady state, in gradual decline, or a lull between episodic global resurfacing events. Worse, even steady-state processes may appear infrequent and episodic on an annual to decadal timescale. To fully understand the behaviour of the Venus lithosphere over time requires geological mapping to ascertain stratigraphic relationships and hence geological history (Hansen 2000), which requires a knowledge of the geological materials at a resolution sufficient to distinguish between stratigraphic units.

3.2. 30 m Reconnaissance Stereo Polarimetric ScanSAR

Radar is sensitive primarily to the morphology (roughness and slope) and relative permittivity of the surface materials. Polarimetric data provide important information about the nature of the surface and near subsurface that cannot be obtained solely with backscatter power images, such as those obtained by Magellan. In particular, polarisation ratios can help identify the thickness and grain size of loose surface sediment (Gaber et al. 2015). Terrestrial studies show that almost all natural targets have reciprocal cross-polarisation, i.e. HV backscatter (horizontally-polarised transmitted waves received as vertically polarised waves) is identical with VH backscatter (Touzi et al. 1993), so that only HH, VV, and VH (or HV) polarisations are required to characterise the backscatter properties. Arecibo data have demonstrated the utility of this at Venus for distinguishing volcanic deposits (Carter et al. 2006), impact ejecta (Campbell et al. 2015) and a thin, patchy but widespread regolith consistent with Venera lander images (Carter et al. 2011), but these data are at a resolution of 12 to 16 km, too low to discern detailed stratigraphic and geological relationships.

VenSAR's polarimetric ScanSAR mode (Figure 8) transmits alternating bursts of horizontal and vertical polarisations, with its single receive channel receiving either H or V polarised echoes. Combinations of these options allows a mix of HH, VH and VV polarised images to be obtained. However, this burst mode of operation causes gain variations (image scalloping) and also degrades the image resolution by a factor of NM + 1, where N is the number of polarisation states, and M, the number of looks taken to mitigate scalloping, typically 2. Because only one of the two cross-polarised images will be acquired the degradation is a factor of 7, enabling a spatial resolution of 30 m.

169 **Figure 8** **Simulated VenSAR Imagery**

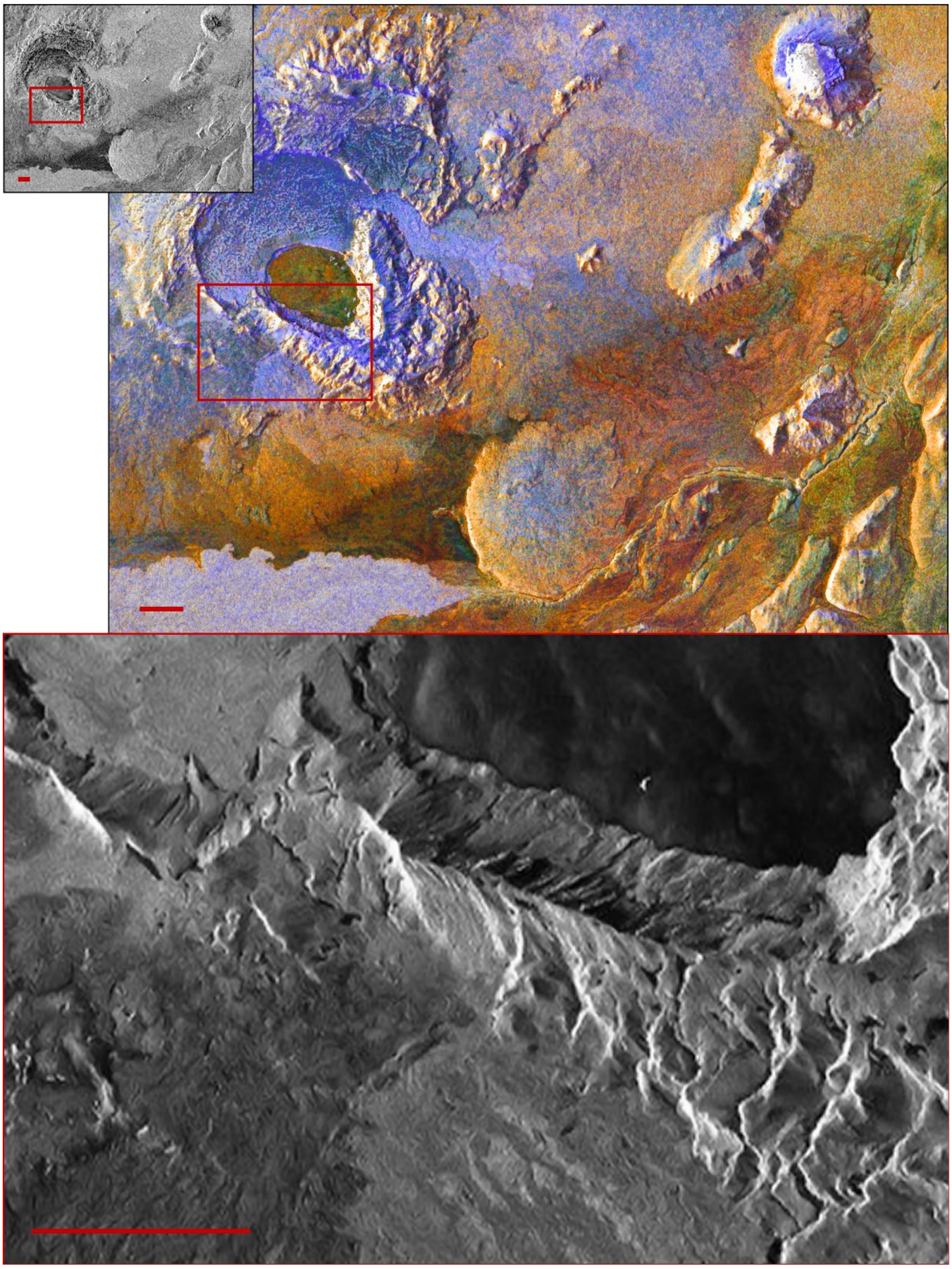

170

Simulated VenSAR image products from Holuhraun, Iceland. Top Left: Simulated Magellan 110 m resolution SAR image (derived from Sentinel 1a data). Notice low contrast from 2-bit BAQ compression and foreshortening due to lack of appropriate DEM. Upper Right: Simulated 30 m resolution HHVHVV StereoPolSAR image (derived from Sentinel 1a data). Note the new lava flow in blue at lower left. Bottom: Simulated 6 m resolution HiRes image (derived from TerraSAR-X data). Scale bar in all images is 2 km.

The InSAR incidence angle (Table 2) is chosen for the optimum phase quality; for polarimetry a higher incidence angle is favoured for its greater sensitivity to surface texture rather than slope. Given this, an angular separation of $\sim$20° has been chosen to allow for the derivation of topography from stereo pairs. Topography from stereo and InSAR are complementary, in the sense that the former is better in steep, rough topography and the latter is better in smooth, gently undulating areas. Both approaches provide for a vertical resolution of $\sim$15 m at a spatial resolution of 90$\sim$120 m. The resolution, swath width and coverage of InSAR and StereoPolSAR data are purposefully compatible to enable provision of contiguous swaths of interferometric, polarimetric and topographic data across 1500 × 1500 km areas for Reconnaissance mapping.

3.3. 6 m Exploration High Resolution Stripmap

Exploration mapping requires 6 m resolution images across selected 100 × 100 km areas. This resolution is achieved in Stripmap mode by increasing the transmit duty ratio (Tx) to bandwidth to 130 MHz – still well within the operating margins – to provide a range resolution of 2 m, which with an azimuth resolution of 3 m, provides for an acceptable 6 looks (Magellan typically had either 5 or 6 looks).

A particular goal for Exploration mapping is the detection of the various lander probes on the Venus surface. The radar cross section of the 2-m diameter Venera landers is approximately 5 dB m^2, giving a normalised radar cross section >20 dB brighter than the background plains, brighter than any natural feature on Venus and readily distinguishable in single look (2 × 3 m) high resolution data. Once located, even higher resolution Locality imaging will be used to confirm their location and characterise the landing sites.

3.4. 1 m Locality Sliding Spotlight

Having identified the brightest single spot within the landing circle, VenSAR will use Sliding Spotlight to image the landing area at 1 m resolution, with less distortion than Staring Spotlight. In Sliding Spotlight, the radar beam is electronically focussed across a single 5 × 5 km area, instead of the normal continuous Stripmap or ScanSAR methods. By adjusting the incidence angle, three or more Sliding Spotlight images may be taken of the same area, allowing for different polarisation states and stereo pairs to fully characterise the site at the metre-scale.

Up to five 5 × 5 km Spotlight scenes may be acquired in any InSAR or StereoPolSAR orbit, on the opposite node. Nearly 450 000 km^2 of allowing for the imaging of many hundreds of different geological features at the Locality scale during the mission, fully meeting the science requirements.

3.5. 5 km Global Passive Radiometry

The relative permittivity of near-surface materials can be inferred from their microwave emissivity, which is derived from the radar brightness temperature of the surface measured by using the SAR antenna as a radiometer. In this mode the resolution is dependent on the real antenna size and hence is very low: ~50 km for Magellan and ~10 km for VenSAR. For most natural materials the relative permittivity depends upon density and can be used to distinguish between areas of loose sediment, weathered rock and exposed fresh rock (Campbell and Ulrichs 1969). Certain materials, e.g. metals, have very high relative permittivity which lowers their emissivity, making these materials very bright in radar imagery. On Venus, slightly elevated relative permittivity can occur in certain volcanic materials, e.g. Ti-rich basalts (Ghail and Wilson 2013); parabolic ejecta halos may have low or moderately elevated relative permittivity (Campbell 1994); and very high relative permittivities occur at high elevations (Arvidson et al. 1994; Pettengill et al. 1992), but not always (Campbell et al. 1999). The cause of these very high relative permittivities is unknown and require polarimetric data, and perhaps observations at different wavelengths, to understand their origin.

VenSAR's receiver and other circuits will remain live throughout each orbit when not actively transmitting (active mode imaging). When the antenna is physically pointed towards nadir for VEM observations, VenSAR will record the brightness temperature of the Venus surface at 3·2 GHz (passive mode), with a precision of ~1 K and a resolution of 4·5 km in azimuth and 38 km in range, a significant improvement on Magellan data. Without additional calibration equipment the absolute accuracy is only ~160 K but because the surface temperature is extremely uniform at a given altitude and the variability is expected to take the form of a small drift (a few K per orbit), the data can be corrected to provide high quality maps of relative emissivity. To improve the absolute accuracy, calibration circuits can be added to provide an absolute brightness temperature accuracy of ~15 K, measured at 2 K precision, at a spatial resolution of 9 km in azimuth and 38 km in range.

4. Remote Control

Unlike Earth Observation satellites, VenSAR is not in a fixed orientation since the spacecraft must be pointed in different orientations for the communications link and for other science experiments. For reliable InSAR, the 3σ pointing requirement is 30 arcsec (0·15 mrad) over 1000 s, and only 250 arcsec (1·2 mrad) over 2800 s for nadir radiometer operations. The advantage of this is that VenSAR can be pointed optimally for each mode; beam steering is not required.

With ascending and descending passes, EnVision passes over every point on the planet twice every Venus day. Normal operations image ahead of the orbit on the ascending node but imaging can also occur on the descending node to investigate changes at ~120 days separation, and behind the orbit (opposite-look) on the ascending node, as is the case for VI3, which provides for 1 to 4 days of time separation for east-west component InSAR and allows for rapid targeting of features of interest at high resolution should, for example, volcanic activity be detected.

The requirement for contiguous data sets of different types places a constraint of a swath width of at least 40 km in order to span the daily 3-orbit, ~6-hour telemetry link. VenSAR is designed to collect 53-km wide swaths to meet this requirement and the additional 10-km baseline between VI1 and VI2. The subsurface sounder will continuously record data along the nadir track while VEM will operate across the night side of Venus only. Radiometry data are also collected on the night side of every mapping orbit except when VenSAR is actively imaging.

The active imaging strategy depends on the Earth-Venus distance, which varies on a 584-day synodic period. InSAR is collected throughout the synodic period but StereoPolSAR and HiRes are obtained only when there is sufficient link capacity. In the 24-hour day shown in Figure 9, VI1 is collected during orbits A, F and K and VI2 (or VI3 after Cycle 1) is collected in orbits B, G and N. No other SAR data would be collected at that time. Orbits C, D, and E are dedicated for telecommunication links but by starting after IS2 on orbit B and ending before IS1 on orbit F, a 5·4 hour link duration is obtained.

Figure 9 **EnVision Mapping Strategy**

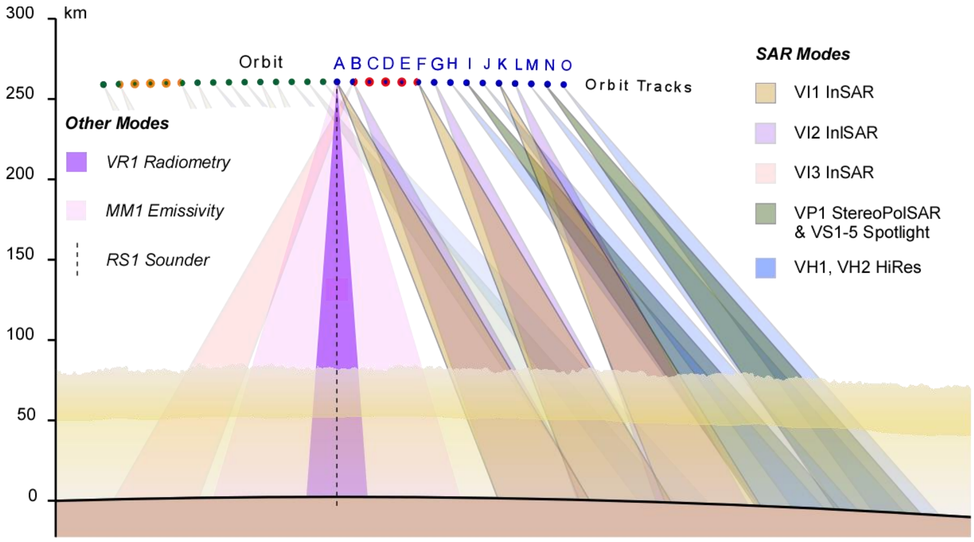

This rather complex figure illustrates the VenSAR mapping sequence for the ~16 orbits in every 24 hours: 4 orbits are reserved for telemetry (open circles); 3 pairs of orbits for InSAR (VI1 and either VI2 or VI3); 2 orbits for StereoPolSAR; and 4 orbits for HiRes and Spotlight. Sounder, Radiometry and VEM data are collected on every mapping orbit; VEM-M and VEM-H on the night side and VEM-U on the day side.

As the link capacity increases, first VP1 data are acquired in orbits I and then N, and then VH1 data in orbits H and J, and then M and O. During these periods, 5 VS1 Sliding Spotlight images are also obtained on each of the InSAR and StereoPolSAR orbits, except for orbit B. The synodic periodicity of high data rates corresponds to 2·4 Venus days, so that every point on the planet will have had both ascending and descending passes after two high data rate peaks. All portions of the planet are thus accessible for high-resolution and polarimetric imaging during the nominal mission.

VenSAR observations will include both contiguous InSAR observations of an equatorial strip and both poles, and targeted observations of regions of interest (ROIs). These are sized to the feature of interest but are typically 1500 × 1500 km (Table 1), equating to ~25 ROIs (~25% of the surface), sufficient to sample and characterise the variety of terranes on Venus. These ROIs will be imaged in every Cycle (Venus day) with IS1 plus IS2 in Cycle 1 and IS1 plus IS3 in every Cycle thereafter. StereoPolSAR coverage of these same regions will be acquired once during the whole mission, first in the latter part of Cycle 1 and the start of Cycle 2, with remaining gaps infilled in Cycle 4 and Cycle 6. Over the same intervals, more than 1400 HiRes 100 × 100 km and 17,500 Spotlight 5 × 5 km scenes will also be obtained within each of the ROIs.

The raw SAR data acquired in all active modes will be losslessly compressed using an optimised block adaptive quantisation method (FD-BAQ), as used on Sentinel-1, reducing the raw data volume by two-thirds (to the values quoted in Table 2), for storage and transmission to Earth.

A key aim for EnVision is to have these compressed raw data returned to Earth in order to form Single Look Complex (SLC) and Ground Range Detected (GRD) products for science distribution. All Level-1 products will be georeferenced and tagged with zero Doppler time at the centre of the swath. Maintenance of these primary data products is vital for research purposes and to allow for future improvements in processing capability and techniques.

5. Conclusions

The VenSAR instrument on EnVision represents a revolution in data quality and volume for a planetary mission, offering an unprecedented view of our nearest planetary neighbour at a quality comparable with Earth Observation data from our own planet. These data will revolutionise our understanding of Venus and provide new insights into the evolution and habitability of Earth-sized exoplanets across the galaxy.

6. References

Anderson, F. Scott and Smrekar, Suzanne E. (2006), 'Global mapping of crustal and lithospheric thickness on Venus', *Journal of Geophysical Research: Planets,* 111 (E8), n/a-n/a.

Arkani-Hamed, Jafar (1993), 'On the tectonics of Venus', *Physics of the Earth and Planetary Interiors,* 76 (1–2), 75-96.

Armann, Marina and Tackley, Paul J. (2012), 'Simulating the thermochemical magmatic and tectonic evolution of Venus's mantle and lithosphere: Two-dimensional models', *Journal of Geophysical Research: Planets,* 117 (E12), n/a-n/a.

Arvidson, R. E., et al. (1994), 'Microwave Signatures and Surface Properties of Ovda Regio and Surroundings, Venus', *Icarus,* 112 (1), 171-86.

Barsukov, V. L., et al. (1986), 'The geology and geomorphology of the Venus surface as revealed by the radar images obtained by Veneras 15 and 16', *Journal of Geophysical Research: Solid Earth,* 91 (B4), 378-98.

Basilevsky, Alexander T. and Head, James W. (1998), 'The geologic history of Venus: A stratigraphic view', *Journal of Geophysical Research: Planets,* 103 (E4), 8531-44.

Berardino, P., et al. (2002), 'A new algorithm for surface deformation monitoring based on small baseline differential SAR interferograms', *IEEE Transactions on Geoscience and Remote Sensing,* 40 (11), 2375-83.

Biggs, Juliet, Anthony, E. Y., and Ebinger, C. J. (2009), 'Multiple inflation and deflation events at Kenyan volcanoes, East African Rift', *Geology,* 37 (11), 979-82.

Bondarenko, N. V., Kreslavsky, M. A., and Head, J. W. (2006), 'North-south roughness anisotropy on Venus from the Magellan Radar Altimeter: Correlation with geology', *Journal of Geophysical Research: Planets,* 111 (E6), E06S12.

Bondarenko, N. V., Head, J. W., and Ivanov, M. A. (2010), 'Present-Day Volcanism on Venus: Evidence from Microwave Radiometry', *Geophysical Research Letters,* 37 (23).

Bonin, B., Bébien, J., and Masson, P. (2002), 'Granite: A Planetary Point of View', *Gondwana Research,* 5 (2), 261-73.

Bullock, Mark A. and Grinspoon, David H. (1996), 'The stability of climate on Venus', *Journal of Geophysical Research: Planets,* 101 (E3), 7521-29.

Butler, B. (2001), 'Accurate and Consistent Microwave Observations of Venus and Their Implications', *Icarus,* 154 (2), 226-38.

Campbell, Bruce A. (1994), 'Merging Magellan Emissivity and SAR Data for Analysis of Venus Surface Dielectric Properties', *Icarus,* 112 (1), 187-203.

--- (1999), 'Surface formation rates and impact crater densities on Venus', *Journal of Geophysical Research: Planets,* 104 (E9), 21951-55.

Campbell, Bruce A., Campbell, Donald B., and DeVries, Christopher H. (1999), 'Surface processes in the Venus highlands: Results from analysis of Magellan and Arecibo data', *Journal of Geophysical Research: Planets,* 104 (E1), 1897-916.

Campbell, Bruce A., et al. (2015), 'Evidence for crater ejecta on Venus tessera terrain from Earth-based radar images', *Icarus,* 250, 123-30.

Campbell, Malcolm J. and Ulrichs, Juris (1969), 'Electrical properties of rocks and their significance for lunar radar observations', *Journal of Geophysical Research,* 74 (25), 5867-81.

Carter, Lynn M., Campbell, Donald B., and Campbell, Bruce A. (2006), 'Volcanic deposits in shield fields and highland regions on Venus: Surface properties from radar polarimetry', *Journal of Geophysical Research,* 111 (E6).

--- (2011), 'Geologic Studies of Planetary Surfaces Using Radar Polarimetric Imaging', *Proceedings of the IEEE,* 99 (5), 770-82.

Chetty, T. R. K., Venkatrayudu, M., and Venkatasivappa, V. (2010), 'Structural architecture and a new tectonic perspective of Ovda Regio, Venus', *Planetary and Space Science,* 58 (10), 1286-97.

Cohen, M. A. B., Lau Semedo, P., and Hall, C. D. (2014), 'Low Cost S-Band SAR Payload for the NovaSAR-S Mission', (ESTEC, Noordwijk: ESA).

DeShon, Heather R., Young, Duncan A., and Hansen, Vicki L. (2000), 'Geologic evolution of southern Rusalka Planitia, Venus', *Journal of Geophysical Research: Planets,* 105 (E3), 6983-95.

Ding, Xiao-li, et al. (2008), 'Atmospheric Effects on InSAR Measurements and Their Mitigation', *Sensors,* 8 (9).

Ferretti, A., Prati, C., and Rocca, F. (2001), 'Permanent scatterers in SAR interferometry', *Geoscience and Remote Sensing, IEEE Transactions on,* 39 (1), 8-20.

Florensky, C. P., Ronca, L. B., and Basilevsky, Alexander T. (1977), 'Geomorphic Degradations on the Surface of Venus: An Analysis of Venera 9 and Venera 10 Data', *Science,* 196 (4292), 869-71.

Florensky, C. P., et al. (1983a), 'Venera 13 and Venera 14: Sedimentary Rocks on Venus?', *Science,* 221 (4605), 57-59.

Florensky, C. P., et al. (1983b), 'Venera 13 and Venera 14: Sedimentary Rocks on Venus?', *Science,* 221 (4605), 57-59.

Ford, Peter G. and Pettengill, Gordon H. (1992), 'Venus topography and kilometer-scale slopes', *Journal of Geophysical Research,* 97 (E8), 13103-03.

Fournier, T. J., Pritchard, M. E., and Riddick, S. N. (2010), 'Duration, magnitude, and frequency of subaerial volcano deformation events: New results from Latin America using InSAR and a global synthesis', *Geochemistry Geophysics Geosystems,* 11 (1).

Fowler, A. C. and O'Brien, S. B. G. (1996), 'A mechanism for episodic subduction on Venus', *Journal of Geophysical Research: Planets,* 101 (E2), 4755-63.

Gaber, Ahmed, et al. (2015), 'Using full-polarimetric SAR data to characterize the surface sediments in desert areas: A case study in El-Gallaba Plain, Egypt', *Remote Sensing of Environment,* 162, 11-28.

Gatelli, F., et al. (1994), 'The wavenumber shift in SAR interferometry', *Geoscience and Remote Sensing, IEEE Transactions on,* 32 (4), 855-65.

Ghail, Richard C. (2002a), 'Structure and evolution of southeast Thetis Regio', *Journal Geophysical Research: Planets,* 107 (E8), 5060-60.

--- (2002b), 'Structure and evolution of southeast Thetis Regio', *J. Geophys. Res.,* 107 (E8), 5060.

--- (2015), 'Rheological and petrological implications for a stagnant lid regime on Venus', *Planetary and Space Science,* 113, 2-9.

Ghail, Richard C. and Wilson, Lionel (2013), 'A pyroclastic flow deposit on Venus', *Geological Society, London, Special Publications,* 401 (1), 97-106.

Ghail, Richard C., Mason, Philippa J., and Skipper, Jacqueline A. (2015), 'The geological context and evidence for incipient inversion of the London', (Edinburgh).

Gilmore, Martha S., et al. (1998), 'Style and sequence of extensional structures in tessera terrain, Venus', *Journal of Geophysical Research: Planets,* 103 (E7), 16813-40.

Grimm, RE and Hess, PC (1997), 'The crust of Venus', *Venus II: Geology, Geophysics, Atmosphere, and Solar Wind Environment* (1), 1205.

Grosfils, Eric B. and Head, James W. (1994), 'The global distribution of giant radiating dike swarms on Venus: Implications for the global stress state', *Geophysical Research Letters,* 21 (8), 701-04.

Guest, John E. and Stofan, Ellen R. (1999), 'A New View of the Stratigraphic History of Venus', *Icarus,* 139 (1), 55-66.

Hansen, V.L. and Young, D.A. (2007), 'Venus's evolution: A synthesis', *Geological Society of America Special Papers,* 419, 255-73.

Hansen, Vicki L. (2000), 'Geologic mapping of tectonic planets', *Earth and Planetary Science Letters,* 176 (3–4), 527-42.

Hashimoto, George L., et al. (2008), 'Felsic highland crust on Venus suggested by Galileo Near-Infrared Mapping Spectrometer data', *Journal of Geophysical Research,* 113.

Hauck, Steven A., Phillips, Roger J., and Price, Maribeth H. (1998), 'Venus: Crater distribution and plains resurfacing models', *Journal of Geophysical Research: Planets,* 103 (E6), 13635-42.

Head, James W., et al. (1992), 'Venus volcanism: Classification of volcanic features and structures, associations, and global distribution from Magellan data', *Journal of Geophysical Research: Planets,* 97 (E8), 13153-97.

Herrick, Robert R. and Rumpf, M. Elise (2011), 'Postimpact modification by volcanic or tectonic processes as the rule, not the exception, for Venusian craters', *Journal of Geophysical Research,* 116 (E2).

Hu, J., et al. (2014), 'Resolving three-dimensional surface displacements from InSAR measurements: A review', *Earth-Science Reviews,* 133, 1-17.

Ivanov, Mikhail A. and Head, James W. (2011), 'Global geological map of Venus', *Planetary and Space Science,* 59 (13), 1559-600.

Jiménez-Díaz, Alberto, et al. (2015), 'Lithospheric structure of Venus from gravity and topography', *Icarus,* 260, 215-31.

Johnson, Catherine L. (2003), 'A conceptual model for the relationship between coronae and large-scale mantle dynamics on Venus', *Journal of Geophysical Research,* 108 (E6).

Jurdy, Donna M. and Stefanick, Michael (1999), 'Correlation of Venus Surface Features and Geoid', *Icarus,* 139 (1), 93-99.

Kargel, Jeffrey S., et al. (1994), 'Carbonate-Sulfate Volcanism on Venus?', *Icarus,* 112 (1), 219-52.

Komatsu, Goro, Gulick, Virginia C., and Baker, Victor R. (2001), 'Valley networks on Venus', *Geomorphology,* 37 (3–4), 225-40.

Lanari, Riccardo, et al. (2007), 'Application of the SBAS-DInSAR technique to fault creep: A case study of the Hayward fault, California', *Remote Sensing of Environment,* 109 (1), 20-28.

Maccaferri, Francesco, Bonafede, M., and Rivalta, Eleonora (2011), 'A quantitative study of the mechanisms governing dike propagation, dike arrest and sill formation', *Journal of Volcanology and Geothermal Research,* 208 (1–2), 39-50.

Malin, Michael C. (1992), 'Mass movements on Venus: Preliminary results from Magellan cycle 1 observations', *Journal of Geophysical Research: Planets,* 97 (E10), 16337-52.

Marcq, Emmanuel, et al. (2013), 'Variations of sulphur dioxide at the cloud top of Venus/'s dynamic atmosphere', *Nature Geosci,* 6 (1), 25-28.

Marov, M.I.A. and Grinspoon, D.H. (1998), *The Planet Venus* (Yale University Press).

Mason, Philippa J., et al. (2015), 'Detecting and monitoring small-scale discrete ground movements across London, using Persistent Scatterer InSAR (PSI)', (Edinburgh).

Massonnet, Didier, et al. (1993), 'The displacement field of the Landers earthquake mapped by radar interferometry', *Nature,* 364 (6433), 138-42.

McCaffrey, K. J. W., et al. (2005), 'Unlocking the spatial dimension: digital technologies and the future of geoscience fieldwork', *Journal of the Geological Society,* 162 (6), 927-38.

McKenzie, Dan, McKenzie, James M., and Saunders, R. Stephen (1992), 'Dike emplacement on Venus and on Earth', *Journal of Geophysical Research: Planets,* 97 (E10), 15977-90.

McKinnon, W. B., et al. (1997), 'Cratering on Venus: Models and observations', in Steven W. Bougher, Donald M. Hunten, and Roger J. Phillips (eds.), (Tucson, Arizona: University of Arizona Press), 969-1014.

Meyer, Franz J. and Sandwell, David T. (2012), 'SAR interferometry at Venus for topography and change detection', *Planetary and Space Science,* 73 (1), 130-44.

Mikhail, Sami (2016), 'A dynamic and testable hypothesis to describe the evolution of the Venusian surface environment', in Colin F. Wilson (ed.), *International Venus Conference* (Oxford), 149-50.

Muhleman, D. (1969), 'Microwave Opacity of the Venus Atmosphere', *The Astronomical Journal,* 74 (1), 57-69.

Nagasawa, Chiaki, Sasaki, Sho, and Koyama, Masato (1998), 'Change of stress field in Beta-Atla-Themis Region on Venus, estimated from surface geometry of dike swarms, lava stratigraphy and crater density', *Geophysical Research Letters,* 25 (22), 4429-32.

Noack, L., Breuer, D., and Spohn, T. (2012), 'Coupling the atmosphere with interior dynamics: Implications for the resurfacing of Venus', *Icarus,* 217 (2), 484-98.

Papuc, Andreea M. and Davies, Geoffrey F. (2012), 'Transient mantle layering and the episodic behaviour of Venus due to the ‘basalt barrier’ mechanism', *Icarus,* 217 (2), 499-509.

Parfitt, E. A. and Head, J. W. (1993), 'Buffered and unbuffered dike emplacement on Earth and Venus: implications for magma reservoir size, depth, and rate of magma replenishment', *Earth, Moon, and Planets,* 61 (3), 249-81.

Pettengill, Gordon H., Ford, Peter G., and Wilt, Robert J. (1992), 'Venus surface radiothermal emission as observed by Magellan', *Journal of Geophysical Research: Planets,* 97 (E8), 13091-102.

Phillips, Roger J., et al. (1992), 'Impact craters and Venus resurfacing history', *Journal of Geophysical Research: Planets,* 97 (E10), 15923-48.

Price, Maribeth H., et al. (1996), 'Dating volcanism and rifting on Venus using impact crater densities', *Journal of Geophysical Research: Planets,* 101 (E2), 4657-71.

Rappaport, Nicole J., et al. (1999), 'An Improved 360 Degree and Order Model of Venus Topography', *Icarus,* 139 (1), 19-31.

Reese, C. C., Solomatov, V. S., and Moresi, L. N. (1998), 'Heat transport efficiency for stagnant lid convection with dislocation viscosity: Application to Mars and Venus', *Journal of Geophysical Research: Planets,* 103 (E6), 13643-57.

--- (1999), 'Non-Newtonian Stagnant Lid Convection and Magmatic Resurfacing on Venus', *Icarus,* 139 (1), 67-80.

Romeo, I. and Capote, R. (2011), 'Tectonic evolution of Ovda Regio: An example of highly deformed continental crust on Venus?', *Planetary and Space Science,* 59 (13), 1428-45.

Romeo, Ignacio, Capote, Ramón, and Anguita, Francisco (2005), 'Tectonic and kinematic study of a strike-slip zone along the southern margin of Central Ovda Regio, Venus: Geodynamical implications for crustal plateaux formation and evolution', *Icarus,* 175 (2), 320-34.

Schepanski, K., Wright, T. J., and Knippertz, P. (2012), 'Evidence for flash floods over deserts from loss of coherence in InSAR imagery', *Journal of Geophysical Research: Atmospheres,* 117 (D20), n/a-n/a.

Seiff, A., et al. (1985), 'Models of the structure of the atmosphere of Venus from the surface to 100 kilometers altitude', *Advances in Space Research,* 5 (11), 3-58.

Shalygin, E. V., et al. (2014), 'Bright Transient Spots in Ganiki Chasma, Venus', *Lunar and Planetary Science,* 45.

Shellnutt, J. Gregory (2013), 'Petrological modeling of basaltic rocks from Venus: A case for the presence of silicic rocks', *Journal of Geophysical Research: Planets,* 118, 1-15.

Simons, Mark, Hager, Bradford H., and Solomon, Sean C. (1994), 'Global Variations in the Geoid/Topography Admittance of Venus', *Science,* 264 (5160), 798-803.

Smrekar, Suzanne E., et al. (2010a), 'Gravity analysis of Parga and Hecate chasmata: Implications for rift and corona formation', *Journal of Geophysical Research: Planets,* 115 (E7), n/a-n/a.

Smrekar, Suzanne E., et al. (2010b), 'Recent Hotspot Volcanism on Venus from VIRTIS Emissivity Data', *Science,* 328 (5978), 605-08.

Smrekar, Suzanne E., et al. (2010c), 'Recent Hotspot Volcanism on Venus from VIRTIS Emissivity Data', *Science,* 328 (5978), 605-08.

Solomatov, V. S. and Moresi, L. N. (1996), 'Stagnant lid convection on Venus', *Journal of Geophysical Research: Planets,* 101 (E2), 4737-53.

Steffes, Paul G., et al. (2015), 'Laboratory measurements of the 3.7–20cm wavelength opacity of sulfur dioxide and carbon dioxide under simulated conditions for the deep atmosphere of Venus', *Icarus,* 245, 153-61.

Stofan, Ellen R., Brian, Antony W., and Guest, John E. (2005), 'Resurfacing styles and rates on Venus: assessment of 18 venusian quadrangles', *Icarus,* 173 (2), 312-21.

Stofan, Ellen R., et al. (1991), 'Corona structures on Venus: Models of origin', *Journal of Geophysical Research: Planets,* 96 (E4), 20933-46.

Stofan, Ellen R., et al. (2001), 'Preliminary analysis of an expanded corona database for Venus', *Geophysical Research Letters,* 28 (22), 4267-70.

Strom, Robert G., Schaber, Gerald G., and Dawson, Douglas D. (1994), 'The global resurfacing of Venus', *Journal of Geophysical Research: Planets,* 99 (E5), 10899-926.

Surkov, Yu A., et al. (1984), 'New data on the composition, structure, and properties of Venus rock obtained by Venera 13 and Venera 14', *Journal of Geophysical Research: Solid Earth,* 89 (S02), B393-B402.

Svedhem, H., et al. (2007), 'Venus as a more Earth-like planet', *Nature,* 450 (7170), 629-32.

Touzi, R., et al. (1993), 'Consideration of antenna gain and phase patterns for calibration of polarimetric SAR data', *IEEE Transactions on Geoscience and Remote Sensing,* 31 (6), 1132-45.

Touzi, R., et al. (1999), 'Coherence estimation for SAR imagery', *IEEE Transactions on Geoscience and Remote Sensing,* 37 (1), 135-49.

Turcotte, D. L., et al. (1999), 'Catastrophic Resurfacing and Episodic Subduction on Venus', *Icarus,* 139 (1), 49-54.

Turcotte, Donald L. (1993), 'An episodic hypothesis for Venusian tectonics', *Journal of Geophysical Research: Planets,* 98 (E9), 17061-68.

Waltham, David A., Pickering, Kevin T., and Bray, Veronica J. (2008), 'Particulate gravity currents on Venus', *Journal of Geophysical Research,* 113 (E2).

Wicks, Charles W., et al. (2006), 'Uplift, thermal unrest and magma intrusion at Yellowstone caldera', *Nature,* 440 (7080), 72-75.

Williams-Jones, Glyn, Williams-Jones, Anthony E., and Stix, John (1998), 'The nature and origin of Venusian canali', *Journal of Geophysical Research: Planets,* 103 (E4), 8545-55.

Woodcock, Curtis E. and Strahler, Alan H. (1987), 'The factor of scale in remote sensing', *Remote Sensing of Environment,* 21 (3), 311-32.

Woodhouse, I. H., Marino, A., and Cameron, I. (2011), 'A standard index of spatial resolution for distributed targets in synthetic aperture radar imagery', *International Journal of Remote Sensing,* 32 (23), 7929-38.

Wright, Tim J. (2004), 'Toward mapping surface deformation in three dimensions using InSAR', *Geophysical Research Letters,* 31 (1).